J. Fluid Mech. (2012), *vol.* 708, *pp.* 279–302.
doi:10.1017/jfm.2012.305

Incompressible impulsive sloshing

Peder A. Tyvand[1]† **and Touvia Miloh**[2]

[1] Department of Mathematical Sciences and Technology, Norwegian University of Life Sciences, P.O. Box 5003, 1432 Ås, Norway

[2] School of Mechanical Engineering, Tel Aviv University, Ramat Aviv 69978, Israel

(Received 29 April 2011; revised 24 February 2012; accepted 17 June 2012; first published online 9 August 2012)

The incompressible impulsive time scale for inviscid liquid sloshing in open rigid containers suddenly put into motion is defined as the intermediate time scale in between the acoustic time scale and the gravitational time scale. Surge and sway boundary-value problems for incompressible impulsive sloshing in some realistic container shapes are solved analytically to the leading order in a small-time expansion. A solution is provided for two types of horizontal cylinders: a triangular cylindrical wedge and a half-filled circular cylinder. The surface velocity and the hydrodynamic force with its corresponding virtual fluid mass are calculated. The cases of constant impulsive velocity and constant impulsive acceleration are linked by transformation equations. Flows with waterline singularities are discussed, being leading-order outer flows in terms of matched asymptotic expansions.

Key words: contact lines, surface gravity waves, wave-structure interactions

1. Introduction

Sloshing of liquids in open containers is an important topic in industrial fluid mechanics. A scientific basis for sloshing is presented in the textbooks by Ibrahim (2005) and Faltinsen & Timokha (2009).

The term sloshing refers to free-surface flows in partially filled containers undergoing motions by external forcing. The importance of initial conditions tends to be underrated in the sloshing literature. There is a need for improved understanding on the initiation of sloshing by putting a container with stagnant fluid impulsively into motion. In general, impulsive sloshing involves interactions between the elasticity of the container and the fluid, where the compressibility of the fluid may also be significant.

This paper is devoted to incompressible impulsive sloshing, which is a well-defined limit case of impulsive sloshing: a rigid container is suddenly forced into motion from an undisturbed state of rest where the incompressible and inviscid liquid has an initial free surface that is horizontal. This abrupt change of motion can either be one of impulsively imposed velocity or impulsively imposed acceleration in the horizontal direction. This type of sloshing is important in earthquake engineering, because all motions start from an undisturbed state at rest. Impulsive forces on dams during earthquakes have been studied by Westergaard (1933), Chwang & Housner (1978) and Chwang (1978). Other applications of incompressible impulsive sloshing include partially filled liquid tanks transported by ships, trains, trucks and missiles. Impulsive

† Email address for correspondence: peder.tyvand@umb.no

sloshing forces should always be taken into account in structural design of open containers in rapidly accelerating systems.

There exist four basic time scales which represent distinct physical processes of transient sloshing within an open rigid container that is put impulsively into steady motion. (i) The acoustic time scale T_{acoust} in the liquid, given by $T_{acoust} = D/c$, where c is the propagation velocity of acoustic waves in the liquid and D is the length scale of the container. The magnitude of T_{acoust} is of the order of milliseconds when D is of the order of 1 m. The acoustic transients will effectively vanish inside a rigid container after a few milliseconds. (ii) The incompressible impulsive time scale T_{incomp} takes over when the acoustic waves in the liquid have disappeared. It is defined indirectly through the intermediate time after the transient acoustic waves have been blurred. (iii) The gravitational time scale $T_{gravity}$, where g is the gravitational acceleration, is given by $T_{gravity} = \sqrt{D/g}$, and is of the order of 0.3 s if D is of the order of 1 m. (iv) Turbulence constitutes a fourth time scale. It is the slowest time scale, provided that the Reynolds number UD/ν is large. Here U is the impulsive velocity of the container and ν is the kinematic viscosity of the liquid. The mechanical energy that is initially given to the fluid will finally decay by small-scale turbulence.

So far, our discussion of the different time scales is limited by the tacit assumption that the characteristic Froude number $F = U/\sqrt{gD}$ is of the order of one or smaller. When $F \gg 1$, an explicit impulsive time scale $T_{incomp} = D/U$ will appear. In this case gravity will never dominate, but it will cause a certain modification of the first stage of sloshing. This first stage ends when the fluid comes to a halt after it hits the end wall of the container. This type of large-Froude-number impulsive sloshing is obviously important in connection with open containers in a low-gravity environment such as in spaceships.

Sloshing can only take place when inertia dominates over viscous forces. This requires that the Reynolds number of the bulk flow is large. Sloshing in rigid containers put into horizontal motion will always have an impulsive stage of incompressible flow, which prevails for all Froude numbers of the free-surface flow in the container.

A classical hydrodynamic problem that is closely related to impulsive sloshing, is the impulsive wavemaker problem. The impulsive wavemaker is a piston (a vertical wall) that is suddenly pushed into a fluid layer at rest (Peregrine 1972). The work by Chwang (1983) fails to take the analysis further, since the nonlinear analysis appears to be incorrect. As noted by Roberts (1988), the classical wavemaker problem is transformed into an impulsive sloshing problem if there are two walls instead of one. A nonlinear analysis of the impulsive wavemaker cannot be done properly before the singularity of the leading-order problem is resolved by matched asymptotic expansion. This has been done for the wavemaker in constant impulsive acceleration (King & Needham 1994) and later for impulsive velocity (Needham, Billingham & King 2007). The logarithmic waterline singularity occurs at a point where the Dirichlet-type free-surface condition and the Neumann-type wall condition are confluent.

Dam-breaking flows lead to similar singularities where the Dirichlet condition of the dam face meets the Neumann condition at the bottom. Again this conflict can be resolved satisfactorily by employing matched asymptotic expansions, see Korobkin & Yilmaz (2009).

We are aware of only two previously published papers on incompressible impulsive sloshing. Chwang & Wang (1984) considered a rectangular container and an upright vertical cylinder. Roberts (1988) provided an alternative method for solving the rectangular container problem. The rectangle problem is two dimensional, with

logarithmic singularities at the waterlines, where the walls meet the free surface. The circular cylinder problem is three dimensional, with antisymmetric waterline singularities along the cylinder wall. The flow inside the geometries considered in these two papers does not discriminate between the two relevant modes of translational motion: surge and sway. In the present work, we will consider two cylindrical geometries where the modes of surge and sway generate different types of flow; those resulting from sway are two-dimensional flows, while those due to surge are three-dimensional flows.

The purpose of the present work is to provide an overview of impulsive sloshing, by generalizing the known solutions and to add some new analytical outer solutions to the existing literature. Thereby we address some important and very challenging problems to be treated by matched asymptotic expansions. Greater care should be taken in developing analytical formulae for sloshing forces, because some of the conventional initial conditions may be physically inconsistent.

2. General mathematical problem in three dimensions

We consider three-dimensional containers with a free surface of liquid at rest for time $t < 0$. The fluid has constant density ρ. The initial free surface is horizontal and the x, y plane is located at the initial free surface. Thus, the undisturbed free surface is defined as $z = 0$. Although the containers that we study are three dimensional, some of the considered flows will be two dimensional. In the present paper we consider only translational impulsive modes of motion. These are the horizontal modes of surge and sway. The third translational mode of vertical impulsive heave is completely disregarded in the present work, since it has no effect on the leading-order linearized flow following immediately after the impulsive start.

The present fluid model is inviscid and incompressible, with the flow starting impulsively from rest. Based on Kelvin's circulation theorem it follows that the flow obeys Laplace's equation

$$\nabla^2 \Phi = 0, \tag{2.1}$$

where $\Phi(x, y, z, t)$ is the velocity potential. We will examine impulsive translational motion of a rigid three-dimensional container. We will consider the two horizontal translational modes of sway motion in the x direction and surge motion in the y direction. An arbitrary initial material point (X_0, Y_0, Z_0) at the rigid container will experience a forced motion $(X(t), Y(t), Z_0)$ prescribed as

$$(X(t), Y(t)) = (X_0, Y_0) + H(t)((X_1, Y_1)t + (X_2, Y_2)t^2 + \cdots) \tag{2.2}$$

where $H(t)$ is the Heaviside unit step function. We will work with two basic cases. First the case of initial impulsive velocity

$$(X_1, Y_1) = (U, V) \tag{2.3}$$

without subsequent acceleration $(X_2 = Y_2 = 0)$. The second case is that of initial impulsive acceleration

$$(2X_2, 2Y_2) \tag{2.4}$$

with zero initial velocity $(X_1 = Y_1 = 0)$.

The general solution for a flow field started by impulsive motion of a rigid container can be expressed by the small-time expansion

$$\Phi(x, y, z, t) = H(t)(\phi_0(x, y, z) + t\phi_1(x, y, z) + t^2\phi_2(x, y, z) + \cdots). \tag{2.5}$$

In our sloshing analysis we will consider constant impulsive velocity started from rest, working with the initial potential $\phi(x, y, z) = \phi_0(x, y, z)$ (dropping the subscript). We will first give transformations linking the case of constant impulsive acceleration to the case of constant impulsive velocity.

The surface elevation $\eta(x, y, t)$ is expressed by a similar small-time expansion

$$\eta(x, y, t) = H(t)(t\eta_1(x, y) + t^2\eta_2(x, y) + \cdots), \tag{2.6}$$

where there is no zeroth-order term because the free surface is initially horizontal:

$$\eta(x, y, 0) = 0. \tag{2.7}$$

Since there is no tangential force on the free surface during the infinitesimal time of the impulsive start, the horizontal velocity at the free surface remains zero. Therefore, the initial free-surface condition is the equipotential condition

$$\Phi(x, y, 0, 0) = 0. \tag{2.8}$$

The exact nonlinear free-surface conditions, ignoring surface tension effects, are given by

$$\frac{\partial \eta}{\partial t} + \nabla\Phi \cdot \nabla\eta = \frac{\partial \Phi}{\partial z}, \quad z = \eta(x, y, t), \tag{2.9}$$

$$\frac{\partial \Phi}{\partial t} + \frac{|\nabla\Phi|^2}{2} + g\eta = 0, \quad z = \eta(x, y, t), \tag{2.10}$$

and the fluid pressure is determined by Bernoulli's equation

$$\frac{p}{\rho} + \frac{\partial \Phi}{\partial t} + \frac{|\nabla\Phi|^2}{2} + gz = 0. \tag{2.11}$$

The net pressure force on the container walls due to the impulsive flow is given by

$$\boldsymbol{F}(t) = \boldsymbol{F}_{-1}\delta(t) + H(t)(\boldsymbol{F}_0 + t\boldsymbol{F}_1 + \cdots), \tag{2.12}$$

where $\delta(t)$ denotes the Dirac delta function and the subscript -1 refers to the instantaneous singular force impulse resulting from the sudden motion of the container.

3. Impulsive velocity and impulsive acceleration

Our investigation is primarily concerned with the case of constant impulsive velocity. Within the present paper we will study only the leading-order outer flow in terms of a small-time matched asymptotic expansion.

First we consider the case of initial impulsive velocity $(X_1, Y_1) = (U, V)$ without subsequent acceleration $(2X_2 = 2Y_2 = 0)$. The resulting leading-order flow is forced by the kinematic wall condition

$$\boldsymbol{n} \cdot \nabla\phi_0 = \boldsymbol{n} \cdot (X_1\boldsymbol{i} + Y_1\boldsymbol{j}), \tag{3.1}$$

where $\boldsymbol{n}$ is the normal vector to the container walls, directed into the fluid. The unit vectors in the x and y directions are denoted by $\boldsymbol{i}$ and $\boldsymbol{j}$, respectively. This initial flow

satisfies the free-surface condition

$$\phi_0(x, y, 0) = 0, \tag{3.2}$$

$$\eta_1 = \left.\frac{\partial \phi_0}{\partial z}\right|_{z=0}, \tag{3.3}$$

with the associated pressure impulse

$$p_{-1} = -\rho\phi_0. \tag{3.4}$$

Integration of this pressure impulse p_{-1} over the container walls will produce the leading-order force $\boldsymbol{F}_{-1}$ for the case of an initial impulsive velocity.

Next, we turn to the case of an initial impulsive acceleration $(2X_2, 2Y_2)$ with zero initial velocity $(X_1 = Y_1 = 0)$. The resulting leading-order flow is given by the kinematic wall condition

$$\boldsymbol{n} \cdot \nabla\phi_1 = 2\boldsymbol{n} \cdot (X_2\boldsymbol{i} + Y_2\boldsymbol{j}), \tag{3.5}$$

with the initial conditions at the free surface

$$\phi_1(x, y, 0) = 0, \tag{3.6}$$

$$2\eta_2 = \left.\frac{\partial \phi_1}{\partial z}\right|_{z=0}. \tag{3.7}$$

The associated zeroth-order pressure is

$$p_0 = -\rho\phi_1. \tag{3.8}$$

Below we will only discuss the first problem of constant impulsive velocity, since the solution for the second case of constant impulsive acceleration can be readily obtained from a set of transformation equations. Let us demonstrate this assertion for the case of forced sway motions of the container in the x direction. The set of variables $(\phi_0, \eta_1, p_{-1}, \boldsymbol{F}_{-1})$ for impulsive sway velocity X_1, is related to the corresponding set of variables $(\phi_1, \eta_2, p_0, \boldsymbol{F}_0)$ for the impulsive sway acceleration $2X_2$, by the following transformation equations

$$\frac{\phi_1}{2X_2} = \frac{\phi_0}{X_1}, \tag{3.9}$$

$$\frac{\eta_2}{X_2} = \frac{\eta_1}{X_1}, \tag{3.10}$$

$$\frac{p_0}{2X_2} = \frac{p_{-1}}{X_1}, \quad \frac{\boldsymbol{F}_0}{2X_2} = \frac{\boldsymbol{F}_{-1}}{X_1}. \tag{3.11}$$

A similar set of transformations link the solutions for impulsive surge velocity Y_1 and impulsive surge acceleration $2Y_2$ in the y direction,

$$\frac{\phi_1}{2Y_2} = \frac{\phi_0}{Y_1}, \tag{3.12}$$

$$\frac{\eta_2}{Y_2} = \frac{\eta_1}{Y_1}, \tag{3.13}$$

$$\frac{p_0}{2Y_2} = \frac{p_{-1}}{Y_1}, \quad \frac{\boldsymbol{F}_0}{2Y_2} = \frac{\boldsymbol{F}_{-1}}{Y_1}. \tag{3.14}$$

It is emphasized that these transformations are only valid for the leading-order outer solution. The initial flow potential, the resulting leading-order elevation and the net

force can then be determined for the case of constant impulsive acceleration, assuming that the solution for constant impulsive velocity is known.

4. Local investigation of waterline singularities

When we combine the wall forcing condition (3.1) with the initial conditions (3.2)–(3.3) at the surface, we find an initial condition preferably written as

$$n_z\eta_1 = \boldsymbol{n}\cdot(X_1\boldsymbol{i}+Y_1\boldsymbol{j}), \quad z=0,\ t=0, \tag{4.1}$$

which holds along the waterline where the container wall and the initial free surface meet. It prescribes the value of the surface velocity η_1 at the waterline expressed by the impulsive container velocity (X_1, Y_1) and the vertical component n_z of the normal vector $\boldsymbol{n}$.

We will now perform a local investigation of the leading-order outer flow near the waterline at $z=0$ where the undisturbed free surface meets the container wall. We assume a constant impulsive velocity, but again the results can be transformed to the case of constant impulsive acceleration. The following investigation is meant to improve our qualitative understanding of the different waterline singularities. It is not a fully precise analysis, since it does not account for the fact that the outer flow problem is elliptic, which means that the local flow near the waterline is not governed exclusively by the local boundary geometry and associated boundary conditions.

Let us assume that the right-hand side of (4.1) is positive. Mass conservation near the wall then implies a locally positive surface velocity $\eta_1 > 0$. There are three different local situations at the waterline, for which we give a simple preliminary analysis based on (4.1).

(i) A sloping wall where $n_z > 0$, which is consistent with the requirement $\eta_1 > 0$. The outer flow is regular, and there is no need for an inner solution.

(ii) A vertical wall where $n_z = 0$, which makes η_1 singular at the waterline $z=0$, as shown by Peregrine (1972) for a piston wavemaker at constant depth. An inner solution is needed to resolve the flow field singularity, but the leading-order force is predicted by the outer solution alone.

(iii) An overhanging wall where $n_z < 0$, which predicts a negative surface velocity η_1 according to (4.1). This result is not significant since it refers to the downward component of the forced wall motion and not to the free-surface velocity.

Tyvand & Storhaug (2000) gave a formula for the local surface velocity generated by a two-dimensional impulsive boundary source of strength q (volume flux per length) that is located at a distance ξ from the waterline, at a slope of angle α

$$\eta_1 = \frac{q}{\alpha\xi}\left(\frac{x}{\xi}\right)^{\pi/(2\alpha)-1}\left(1+\left(\frac{x}{\xi}\right)^{\pi/\alpha}\right)^{-1}, \quad z=0,\ t=0. \tag{4.2}$$

In order to study the local behaviour near the waterline $x=0$, let us first assume that the source position ξ has a given finite value, and let $x\to 0$. We can then take the limit $x/\xi \ll 1$ of (4.2), which gives η_1 proportional to $x^{\pi/(2\alpha)-1}$. Again we have the three cases described previously.

(i) A sloping wall where $n_z > 0$ and $0 < \alpha < \pi/2$. The surface velocity varies as a positive power of x. The free-surface flow (4.2) has no singularity, and indicates that the fluid is stagnant at the waterline $x=0$.

(ii) A vertical wall where $n_z = 0$ and $\alpha = \pi/2$. The surface elevation is independent of x for small x.

(iii) An overhanging wall where $n_z < 0$ and $\pi/2 < \alpha < \pi$. The surface velocity varies as a negative power of x. There is a waterline singularity at $x = 0$, which becomes increasingly severe the greater the angle α.

Our arguments do not explain, however, the free-surface behaviour when the wall performs a locally uniform impulsive motion. In this case we would need to integrate (4.2) with respect to ξ up to $\xi = 0$. This means that the assumption $x/\xi \ll 1$ of the previous discussion cannot be maintained, which may in fact modify the behaviour in all three cases (i)–(iii) as follows.

(i) For a sloping wall where $n_z > 0$ and $0 < \alpha < \pi/2$, the fluid set into motion by a piston in impulsive motion of uniform translation is not necessarily stagnant at the waterline. Below we will show such an example: a wedge container put into sway motion that generates finite velocity at the waterline.

(ii) For a vertical wall where $n_z = 0$ and $\alpha = \pi/2$, the surface velocity near the waterline is no longer independent of x when we have finite source contributions in the limit $\xi \to 0$. Peregrine (1972) demonstrated the existence of a logarithmic singularity for the surface velocity due to a uniform impulsive wavemaker. The geometry is also different for the piston wavemaker, since the latter works at a constant water depth H. It is important to note that the depth H for the piston wavemaker in the vertical direction determines the horizontal length scale for the impulsive free-surface flow. It can also be shown that an impulsive pitch rotation of the piston wavemaker will give a finite surface velocity at the waterline.

(iii) For an overhanging wall, where $n_z < 0$ and $\pi/2 < \alpha < \pi$, the surface velocity is singular in x with the local dependence $x^{\pi/(2\alpha)-1}$ near the waterline. This singularity becomes more severe with increasing α, but remains mild for slightly overhanging walls. Actually Needham, Chamberlain & Billingham (2008) have shown that the resulting free surface flow will be regular over the interval $0.5 < \alpha/\pi < 0.570$, where the overhanging wall has a finite extent as the face of the wavemaker is operating at constant depth.

Our mathematical formulation is an outer problem in the matched asymptotics sense, and the solutions (including the waterline singularities) may provide consistent outer solutions. No work has been reported on the matched asymptotics of incompressible impulsive sloshing, as the two published papers (Chwang & Wang 1984; Roberts 1988) are only concerned with the outer solutions.

In comparison, matched asymptotic expansions have been developed for some related two-dimensional piston-type wavemaker problems. First for the case of constant impulsive acceleration (King & Needham 1994), later for constant impulsive velocity (Needham *et al.* 2007) and finally for the case of a sloping-face wavemaker (Needham *et al.* 2008). Waterline singularities of a logarithmic nature are also known to appear in the typical three-dimensional nonlinear diffraction of water waves around vertical cylinders standing in water of finite depth (Miloh 1980).

5. A wedge container

The first problem that we solve is that of a rigid wedge composed of two sloping walls at angles $\pm\pi/4$, combined with two vertical end-walls at $y = 0$ and $y = L$. The two slopes of the wedge are defined by $z = -x$ and $z = x - 2H$. The depth of the wedge is H, which implies that its width in the x direction is $2H$ when filled with fluid at rest. The undisturbed free surface ($z = 0$) encompasses the rectangle $0 \leqslant x \leqslant 2H$, $0 \leqslant y \leqslant L$. The fluid mass within the wedge container is $m = \rho H^2 L$. See the perspective sketch in figure 1.

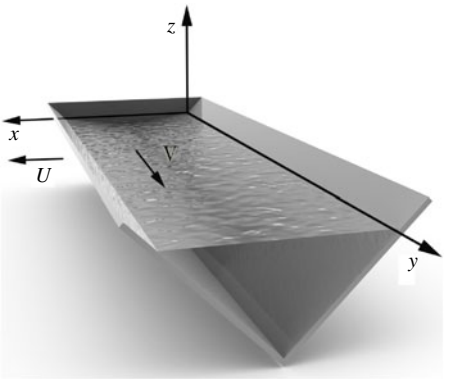

FIGURE 1. Perspective sketch of a wedge container with undisturbed fluid. The container can be put into impulsive sway motion with velocity U in the x direction. It can be put into impulsive surge motion with velocity V in the y direction.

5.1. *The two-dimensional sway problem for the wedge*

We consider the impulsive sway motion with velocity U in the cross-wise x direction, which produces a two-dimensional flow in the x, z plane, with normal velocity $\mp U/\sqrt{2}$ on the two slopes. The resulting velocity potential is

$$\phi(x, z) = U\left(1 - \frac{x}{H}\right) z, \tag{5.1}$$

with the associated stream function

$$\psi(x, z) = U\frac{x^2 - z^2}{2H} - Ux. \tag{5.2}$$

The leading-order surface velocity is

$$\eta_1 = \left.\frac{\partial \phi}{\partial z}\right|_{z=0} = U\left(1 - \frac{x}{H}\right). \tag{5.3}$$

This leading order is exceptionally simple, as the free surface evolves with a uniform slope. Two streamline patterns for the initial sway flow are given in figure 2. The first streamline pattern has a coordinate system that is at rest with the undisturbed fluid. It is characterized by vertical particle motion at the free surface. The second streamline pattern takes the container in its motion as a reference system, and the streamlines are tangential to the container walls.

The streamlines in the system that follow the container in its motion, could be taken as the redefined container walls. These streamlines form a family of hyperbolas, and their common asymptotes represent the contour of the wedge container.

The total net impulsive sway force on the two slopes is thus given by

$$F_{-1x} = -\tfrac{1}{3}\rho H^2 L U = -\tfrac{1}{3} m U. \tag{5.4}$$

This formula demonstrates that the virtual mass of a wedge container in impulsive sway is one third of the enclosed fluid mass. Physically, this means that an open wedge container in sway motion that is suddenly brought to a halt can effectively only stop one third of the fluid mass instantaneously. Owing to inertia, the remaining two thirds of the fluid mass will continue its sway motion relative to the container, thereby delaying and distributing over time its total impact force on the container.

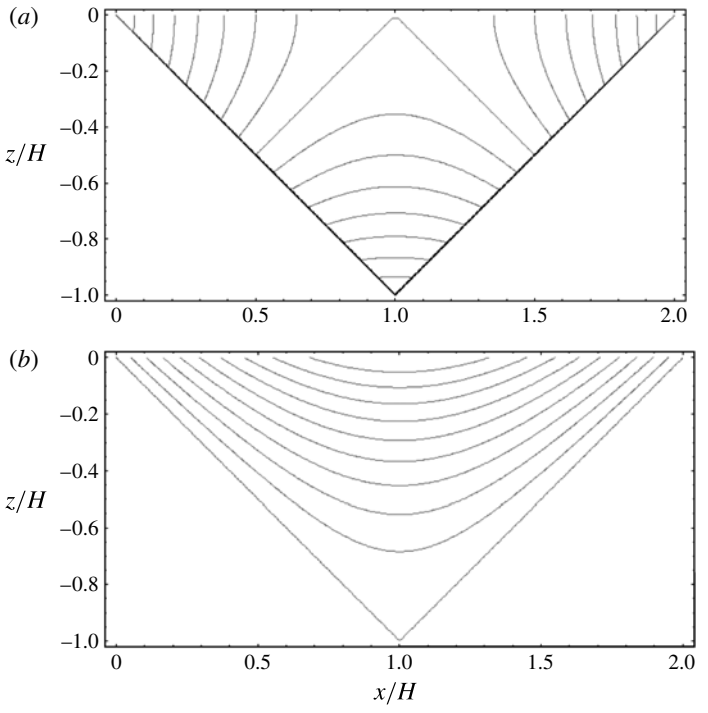

FIGURE 2. Streamline patterns for the two-dimensional impulsive sway flow in the wedge container. (*a*) The coordinate system is at rest with respect to the undisturbed fluid. (*b*) The coordinate system follows the container in its impulsive motion.

5.2. *The three-dimensional surge problem for the wedge*

An impulsive motion of the wedge container with velocity V in the lengthwise y direction will generate a three-dimensional flow. We will derive the velocity potential for this case in terms of a Fourier series. The normal velocity on the wall $y = 0$, in combination with the impermeability condition along both slopes as well as the equipotential free-surface condition, gives the following Fourier expansion in the fluid domain;

$$\left.\frac{\partial\phi}{\partial y}\right|_{y=0,L} = V = -\frac{16}{\pi^2}V\sum_{m=1}^{\infty}\frac{\sin\left(\left(m-\frac{1}{2}\right)\frac{\pi x}{H}\right)}{2m-1}\sum_{n=1}^{\infty}\frac{\sin\left(\left(n-\frac{1}{2}\right)\frac{\pi z}{H}\right)}{2n-1}, \quad (5.5)$$

where the slope boundary conditions of zero normal velocity are taken into account. The leading-order solution for the surface velocity is

$$\eta_1 = \left.\frac{\partial\phi}{\partial z}\right|_{z=0} = \frac{8V}{\pi^2}\sum_{m=1}^{\infty}\frac{\sin\left(\left(m-\frac{1}{2}\right)\frac{\pi x}{H}\right)}{2m-1} \times \sum_{n=1}^{\infty}\frac{\cosh\left(\frac{\pi(y-L)}{H}\sqrt{\left(m-\frac{1}{2}\right)^2+\left(n-\frac{1}{2}\right)^2}\right)-\cosh\left(\frac{\pi y}{H}\sqrt{\left(m-\frac{1}{2}\right)^2+\left(n-\frac{1}{2}\right)^2}\right)}{\sqrt{\left(m-\frac{1}{2}\right)^2+\left(n-\frac{1}{2}\right)^2}\sinh\left(\frac{\pi L}{H}\sqrt{\left(m-\frac{1}{2}\right)^2+\left(n-\frac{1}{2}\right)^2}\right)}. \quad (5.6)$$

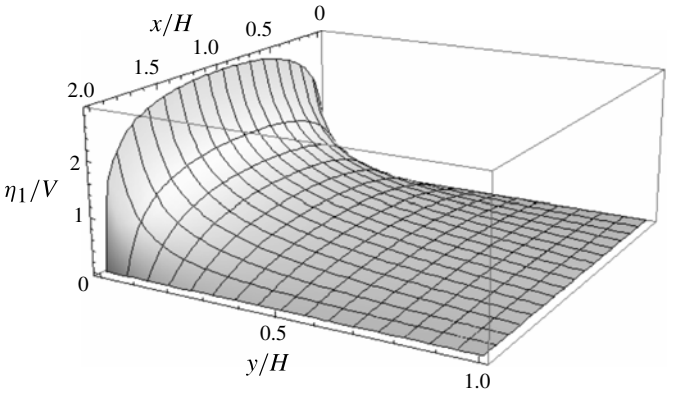

FIGURE 3. Surface velocity distribution $\eta_1(x, y)$ for the three-dimensional impulsive surge flow in a wedge container with aspect ratio $L/H = 2$. The figure covers the full domain $0 < x/H < 2$ in the x direction and almost half the domain $0.001 < y/H < 1$ in the y direction.

Figure 3 shows the surface velocity distribution $\eta_1(x, y)/V$ over the free surface for the case $L/H = 2$. We show only half the fluid domain, because the flow is antisymmetric around $y = L/2$. Owing to the waterline singularity, the convergence and accuracy of the truncated Fourier series solution is relatively slow close to the end-wall waterline $y = 0$.

The net impulsive force exerted on the two end walls is proportional to the area integral of the potential

$$F_{-1y} = 2\rho \int_A \phi(x, 0, z)\, \mathrm{d}A = 2\rho \int_{-H}^{0} \left(\int_{-z}^{2H+z} \phi(x, 0, z)\, \mathrm{d}x \right) \mathrm{d}z$$
$$= \frac{64\rho V H^3}{\pi^5} \sum_{m=1}^{\infty} \sum_{n=1}^{\infty} \frac{2n - 1 - (2m-1)\,(-1)^{m+n}}{(m-n)(m+n-1)(2n-1)\,(2m-1)^2}$$
$$\times \frac{\tanh\left(\dfrac{\pi L}{2H} \sqrt{\left(m - \dfrac{1}{2}\right)^2 + \left(n - \dfrac{1}{2}\right)^2} \right)}{\sqrt{\left(m - \dfrac{1}{2}\right)^2 + \left(n - \dfrac{1}{2}\right)^2}}. \tag{5.7}$$

In order to evaluate this force correctly, one should note that for $m = n = l$ the argument in the double summation is finite and equals

$$\frac{2^{3/2} \tanh\left(\dfrac{\pi L}{2^{3/2} H} (2l - 1) \right)}{(2l-1)^5}. \tag{5.8}$$

The dimensionless force impulse $F_{-1y}/(\rho H^3 V)$ is defined with respect to the momentum of a fluid cube with side length H put into motion with velocity V. The limit for this dimensionless force impulse as $L/H \to \infty$ is $F_{-1y}/(\rho H^3 V) \to -0.3833$, which can be found by numerical evaluation of (5.7). This result can be interpreted

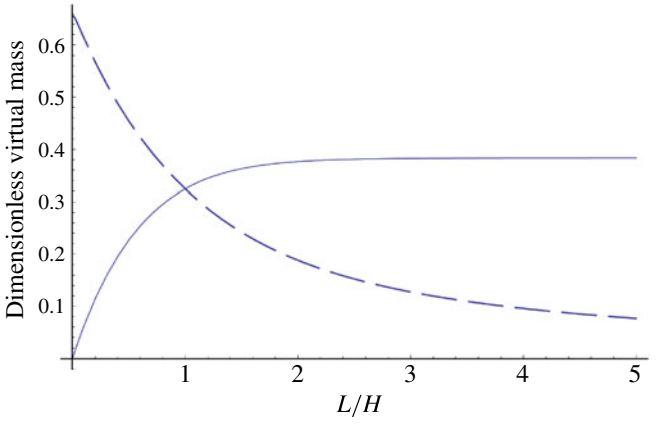

FIGURE 4. (Colour online) Two versions of the dimensionless virtual mass for surge motion of the wedge container, displayed as functions of the aspect ratio L/H. The solid curve represents $F_{-1y}/(\rho H^3 V)$. The dashed curve represents $F_{-1y}/(\rho H^2 LV)$.

as a local momentum thickness of $0.1917H$ close to each end-wall for an extremely long container. Only the fluid inside the two momentum layers will effectively follow the container in its impulsive motion. This is in contrast to the fluid outside the layers, which by inertia will continue its motion unaffected by the abrupt motion of the container end-walls. The trivial limit for this dimensionless force impulse $F_{-1y}/(\rho H^3 V)$ as $L/H \to 0$ is zero, since the fluid mass vanishes.

A complimentary way of displaying the dimensionless force impulse is as $F_{-1y}/(mV) = F_{-1y}/(\rho H^2 LV)$. This formulation represents the ratio between the virtual mass for impulsive surge motion and the fluid mass inside the wedge. In figure 4 we show the two dimensionless versions of the impulsive force, $F_{-1y}/(\rho H^3 V)$ and $F_{-1y}/(\rho H^2 LV)$, as functions of L/H, according to (5.7). An obvious but trivial limit for the second version of the dimensionless force impulse is $F_{-1y}/(\rho H^2 LV) \to 0$ as $L/H \to \infty$. A notable special case occurs when $L/H = 0.9578$, in which we have

$$\frac{|F_{-1y}|}{mV} = \frac{|F_{-1x}|}{mU} = \frac{1}{3} \tag{5.9}$$

implying that the virtual mass is a scalar that equals $m/3$. When $L/H > 0.9578$, the surge virtual mass is smaller than the sway virtual mass, and when $L/H < 0.9578$, the situation is reversed.

The dimensionless force impulse has an interesting limit $F_{-1y}/(\rho H^2 LV) \to -0.666$ as $L/H \to 0$. This result implies that the ratio between the virtual and the fluid masses for the surge motion of a short wedge is twice as large as the value $1/3$ that is obtained for the sway motion. The reason for this difference is that the fluid flow is more restricted in surge than in sway: it is easier to force a fluid with a free surface to follow the motion of a vertical boundary than that of a sloping one. Furthermore, fluid motion in surge has the extra constraint that the free-surface flow vanishes at the lateral waterlines, implying that the resulting three-dimensional free-surface flow must be concentrated around the middle where the water depth of the wedge is maximal.

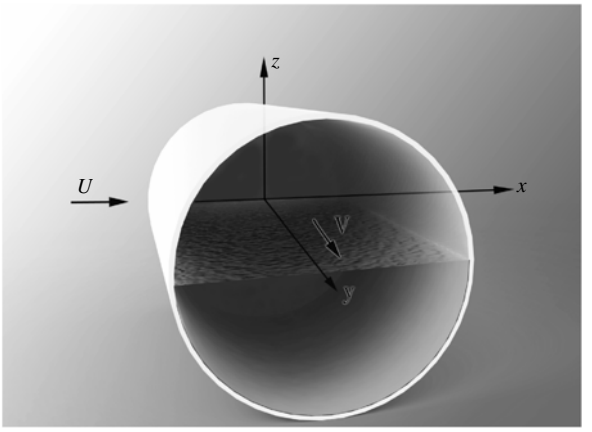

FIGURE 5. Perspective sketch of a horizontal cylinder with a circular cross-section, half-filled with fluid. The container can be put into impulsive sway motion with velocity U in the x direction. It can be put into impulsive surge motion with velocity V in the y direction.

6. The half-filled horizontal circular cylinder

The impulsive flow inside a rigid half-filled horizontal cylinder will now be solved. See the perspective sketch in figure 5. The y-axis is directed along the centre of the cylinder and its vertical end-walls are located at $y = 0, L$. The undisturbed free surface ($z = 0$) covers the rectangle $-R \leqslant x \leqslant R$, $0 \leqslant y \leqslant L$. The circular cross-section of the cylinder is given by $x^2 + z^2 = R^2$, where R is the radius of the cylinder. We introduce polar coordinates (r, θ) in the x, z plane, defined by $(x, z) = r(\cos\theta, \sin\theta)$. The initially filled lower half of the cylinder covers $\pi < \theta < 2\pi$ and $0 \leqslant r < R$.

6.1. *The two-dimensional sway problem for the horizontal cylinder*

We first consider an impulsive sway motion with velocity U in the cross-wise x direction. The normal velocity along the bottom is represented by the boundary condition

$$\frac{\partial \phi}{\partial r} = U\cos\theta, \quad r = R \ (\pi < \theta < 2\pi). \tag{6.1}$$

The initial free-surface condition $\phi = 0$ at $z = 0$ is conveniently satisfied by applying an antisymmetric image condition along the upper (dry) part of the cylinder contour

$$\frac{\partial \phi}{\partial r} = -U\cos\theta, \quad r = R(0 < \theta < \pi). \tag{6.2}$$

The solution to this two-dimensional problem in terms of the potential and stream function is

$$\phi(r, \theta) + i\psi(r, \theta) = \frac{4iUR}{\pi} \sum_{n=1}^{\infty} \frac{(r/R)^{2n}\, \mathrm{e}^{2in\theta}}{4n^2 - 1}. \tag{6.3}$$

The resulting free-surface velocity is

$$\eta_1 = \left.\frac{\partial \phi}{\partial z}\right|_{z=0} = \left.\frac{1}{r}\frac{\partial \phi}{\partial \theta}\right|_{\theta=0} = -\frac{8U}{\pi} \sum_{n=1}^{\infty} \frac{n}{4n^2 - 1} \left(\frac{x}{R}\right)^{2n-1}, \tag{6.4}$$

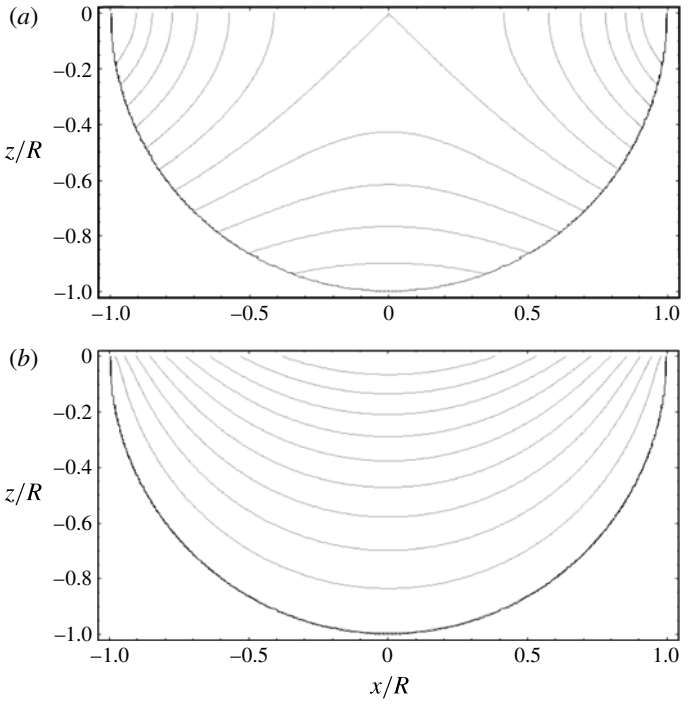

FIGURE 6. Streamline patterns for the two-dimensional impulsive sway flow in the half-filled horizontal cylinder. (*a*) The coordinate system is at rest with respect to the undisturbed fluid. (*b*) The coordinate system follows the container in its impulsive motion.

valid for $-R < x < R$. We note the presence of a logarithmic singularity in the surface velocity that arises at the waterlines $x = \pm R$. Two streamline patterns for the initial sway flow are given by (6.3) and displayed in figure 6. The first has a coordinate system that is at rest with the undisturbed fluid. It is characterized by vertical particle motion at the free surface. The second streamline pattern takes the container in its motion as a reference system, and the streamlines are tangential to the container walls. It is interesting to compare the streamline patterns in figure 6 with those for the wedge container, given in figure 2. For the circular cylinder, the flow is more concentrated near the waterlines. This is because the sway flow inside the cylinder is singular at the waterlines, in contrast to the wedge container.

The streamlines in the reference system that follow the container in its motion may be redefined to form modified container cross-sections. All of these redefined containers have approximate circle sections. All of them cover less than half a circle, which means that they have finite slopes at the waterlines, which implies non-singular flows. The half-circle cross-section is the only exception, as its vertical tangent at the waterline leads to a logarithmic singularity there.

In figure 7 we compare the two-dimensional surface velocity distribution (6.4) for a cylinder in sway motion with the sway (5.3) and surge (5.6) surface velocities for a wedge of length $L = 2H$. Little difference is observed between these three solutions near the middle of the free surface. However, close to the walls of the container the presence of flow singularities is very important.

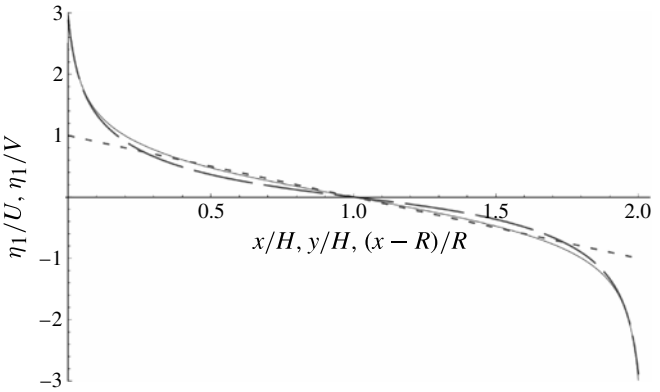

FIGURE 7. Comparison of three free-surface velocity distributions. Dotted curve: $\eta_1(x)/U$ for the two-dimensional sway motion of the wedge. Dashed curve: central surface velocity $\eta_1(H, y)/V$ for the surge motion of a wedge with length $L = 2H$. Solid curve: $\eta_1(x - R)/U$ for the two-dimensional sway motion of the half-filled circular cylinder.

The net impulsive sway force acting on the half cylinder is given by

$$F_{-1x} = -2\rho LR \int_{-\pi/2}^{0} \phi(R, \theta) \cos\theta \, \mathrm{d}\theta$$
$$= -\frac{16}{\pi} \rho LR^2 U \sum_{n=1}^{\infty} \frac{n}{(4n^2 - 1)^2} = -\frac{4}{\pi^2} mU, \tag{6.5}$$

where we have introduced the fluid mass $m = \rho\pi R^2 L/2$. This formula shows that the ratio between the virtual mass and the fluid mass for a half-filled horizontal cylinder put impulsively into sway is $4/\pi^2 = 0.4053$.

6.2. *The three-dimensional surge problem for the horizontal cylinder*

We now turn our attention to the more complicated case of impulsive surge motion with velocity V in the y direction, along the axis of the half-filled horizontal cylinder. The horizontal surge motion requires a uniform normal velocity V over the wet part of the vertical end-walls $x = 0, L$. Expressed in cylindrical coordinates (r, θ, y) this gives the normal flow condition

$$\frac{\partial \phi}{\partial y}(r, \theta, 0) = \frac{\partial \phi}{\partial y}(r, \theta, L) = V, \quad r < R, \ \pi < \theta < 2\pi. \tag{6.6}$$

In order to satisfy the equipotential condition at $z = 0$ $(\theta = 0, \pi)$, we will apply an image condition along the dry portions of the end-walls. Extension of this condition to the dry part of the cylinder yields the general boundary condition for the impermeable walls as

$$\frac{\partial \phi}{\partial r}(R, \theta, y) = 0, \quad 0 < y < L, \ 0 < \theta < 2\pi. \tag{6.7}$$

Using the method of successive images, let us express the velocity potential in Cartesian coordinates as

$$\phi(x, y, z) = -\frac{V}{2\pi} \sum_{m=-\infty}^{\infty} (-1)^m (G(x, y - mL, z) + H(x, y - mL, z)). \tag{6.8}$$

Equation (6.8) is basically a Green function solution, where G accounts for the boundary conditions at the end-walls and free surface, and H provides the necessary adjustment required to satisfy the impermeable cylinder wall condition (6.7). Here $G(x, y - mL, z)$ summed over all integer values of m represents an infinite row of uniform distributions of sources/sinks over the wet areas S_w of the end walls. It can be expressed in a Fourier–Bessel form as

$$\begin{aligned} G(x, y - mL, z) &= \int_{S_w} \frac{\mathrm{d}\xi\, \mathrm{d}\zeta}{\sqrt{(x-\xi)^2 + (y - mL)^2 + (z-\zeta)^2}} \\ &\quad - \int_{S_w} \frac{\mathrm{d}\xi\, \mathrm{d}\zeta}{\sqrt{(x-\xi)^2 + (y - mL)^2 + (z+\zeta)^2}} \\ &= \frac{2}{\pi} \int_{S_w} \left(\int_0^\infty \left(\mathrm{K}_0(k\sqrt{(x-\xi)^2 + (z-\zeta)^2}) \right.\right. \\ &\quad \left.\left. - \mathrm{K}_0\left(k\sqrt{(x-\xi)^2 + (z+\zeta)^2}\right)\right) \cos(k(y - mL))\, \mathrm{d}k \right) \mathrm{d}\xi\, \mathrm{d}\zeta, \end{aligned} \tag{6.9}$$

see Miloh, Tyvand & Zilman (2002). The modified Bessel function of the second kind is denoted by K_n, and J_n denotes the Bessel function of the first kind (order n). Next we use the following addition theorem (Abramowitz & Stegun 1965, p. 363)

$$\begin{aligned} &\mathrm{K}_0(k\sqrt{(x-\xi)^2 + (z-\zeta)^2}) - \mathrm{K}_0(k\sqrt{(x-\xi)^2 + (z+\zeta)^2}) \\ &\quad = 4 \sum_{n=1}^{\infty} \sin(n\theta) \sin(n\alpha) \begin{cases} \mathrm{J}_n(k\lambda)\mathrm{K}_n(kr), & r > \lambda, \\ \mathrm{J}_n(kr)\mathrm{K}_n(k\lambda), & r < \lambda. \end{cases} \end{aligned} \tag{6.10}$$

Here we have introduced the polar coordinates (λ, α) for the source position $(\xi, \zeta) = \lambda(\cos\alpha, \sin\alpha)$. Substituting (6.10) into (6.9) and integrating over $S_w (0 < \lambda < R, \pi < \alpha < 2\pi)$ yields

$$\begin{aligned} G(x, y - mL, z) &= -\frac{16}{\pi} \sum_{n=0}^{\infty} \frac{\sin((2n+1)\theta)}{2n+1} \\ &\quad \times \int_0^\infty F(k, n, r, R) \cos(k(y - mL))\, \mathrm{d}k, \end{aligned} \tag{6.11}$$

where $(x, y) = r(\cos\theta, \sin\theta)$, and the function $F(k, n, r, R)$ is defined by

$$F(k, n, R, r) = \mathrm{K}_n(kr) \int_0^r \lambda \mathrm{J}_n(k\lambda)\, \mathrm{d}\lambda + \mathrm{J}_n(kr) \int_r^R \lambda \mathrm{K}_n(k\lambda)\, \mathrm{d}\lambda. \tag{6.12}$$

It can be easily verified from (6.9) that G is indeed harmonic, satisfying $\partial G/\partial y = -2\pi$ on $y = 0, L$ and that $G(x, y - mL, 0) = 0$ on the initial free surface. In order to satisfy the cylinder wall condition $\partial G/\partial r(R, \theta, y) = 0$, the regular harmonic function H introduced in (6.8) is expressed by virtue of (6.11) as

$$\begin{aligned} H(x, y - mL, z) &= -\frac{16}{\pi} \sum_{n=0}^{\infty} \frac{\sin((2n+1)\theta)}{2n+1} \\ &\quad \times \int_0^\infty A(k, n, R) \mathrm{I}_{2n+1}(kr) \cos(k(y - mL))\, \mathrm{d}k, \end{aligned} \tag{6.13}$$

where I_n denotes the modified Bessel function of the first kind and $A(k, m, R)$ is to be determined. The regular function (6.13) satisfies the free-surface boundary condition $H(x, y - mL, 0) = 0$ (for $\theta = \pi, 2\pi$). When summing over all m, it is clear that $\partial H/\partial y = 0$ on $y = 0, L$. The unknown factor $A(k, n, R)$ can then be determined by imposing the requirement of zero normal derivative at $r = R$, which by virtue of (6.8) gives

$$\frac{\partial H}{\partial r} = -\frac{\partial G}{\partial r} \quad \text{for } r = R. \tag{6.14}$$

Differentiating and inserting the above expressions for G and H gives

$$A(k, n, R) = \frac{\mathrm{K}'_{2n+1}(kR)}{\mathrm{I}'_{2n+1}(kR)} \int_0^R \lambda \mathrm{J}_{2n+1}(k\lambda)\, \mathrm{d}\lambda, \tag{6.15}$$

where the prime denotes the derivative with respect to the argument. Thus, the final solution for the velocity potential induced by surge motion of a half-filled horizontal cylinder can be expressed as

$$\begin{aligned}\phi(x, y, z) = -\frac{V}{2\pi} \sum_{m=-\infty}^{\infty} (-1)^m \int_{S_w} \left(\frac{1}{\sqrt{(x-\xi)^2 + (y - mL)^2 + (z-\zeta)^2}} \right. \\ \left. - \frac{1}{\sqrt{(x-\xi)^2 + (y - mL)^2 + (z+\zeta)^2}} \right) \mathrm{d}\xi\, \mathrm{d}\zeta \\ + \frac{8V}{\pi^2} \sum_{n=0}^{\infty} \sum_{m=0}^{\infty} \epsilon_m \frac{\sin((2n+1)\theta)}{2n+1} \\ \times \int_0^{\infty} A(k, n, R) \mathrm{I}_{2n+1}(kr) \cos(ky) \cos(kmL)\, \mathrm{d}k \end{aligned} \tag{6.16}$$

where $\epsilon_0 = 1$ and $\epsilon_n = 2$ for $n \neq 0$.

It is cumbersome numerically to integrate up the full solution (6.16) for a cylinder of finite length L. Here we will therefore consider only the limit $L/R \to \infty$ and calculate the force F_{-1y} acting on one end-wall $y = 0$. For a very long but finite cylinder, there will be an equal impulsive force on the other end-wall $y = L$, so that the total force will be $2F_{-1y}$. The impulsive hydrodynamic force on the single end-wall $y = 0$ of a half-filled semi-infinite horizontal cylinder is thus

$$F_{-1y} = \rho \int_0^{\pi} \int_0^R r\phi(r, 0, \theta)\, \mathrm{d}r\, \mathrm{d}\theta = (C_1 + C_2)\rho V R^3. \tag{6.17}$$

The coefficient C_1 represents the contribution from the source distribution plus its image (the Green function) and the correction C_2 takes care of the adjustment to the boundary condition at the end wall $y = 0$. We choose to evaluate C_1 directly in Cartesian coordinates as

$$\begin{aligned} C_1 = \frac{1}{2\pi} \int_{-1}^{1} \int_{-1}^{1} \int_{-\sqrt{1-x^2}}^{0} \int_{-\sqrt{1-\xi^2}}^{0} \\ \times \left(\frac{\mathrm{d}x\, \mathrm{d}\xi\, \mathrm{d}z\, \mathrm{d}\zeta}{\sqrt{(x-\xi)^2 + (z+\zeta)^2}} - \frac{\mathrm{d}x\, \mathrm{d}\xi\, \mathrm{d}z\, \mathrm{d}\zeta}{\sqrt{(x-\xi)^2 + (z-\zeta)^2}} \right). \end{aligned} \tag{6.18}$$

The integrations with respect to z and ζ are performed analytically by Mathematica and the resulting double integral is evaluated numerically to yield $C_1 = -0.48444$.

Inserting the contribution $m = 0$ from the general solution (6.16), we find after some algebra the following expression for C_2

$$C_2 = \frac{16}{\pi^2} \sum_{n=0}^{\infty} (2n+1)^{-2} \int_0^{\infty} \frac{\mathrm{K}'_{2n+1}(k)}{\mathrm{I}'_{2n+1}(k)} P_{2n+1}(k) Q_{2n+1}(k) k^{-4} \, \mathrm{d}k, \tag{6.19}$$

where

$$P_{2n+1}(k) = \int_0^k t \mathrm{J}_{2n+1}(t) \, \mathrm{d}t, \tag{6.20}$$

$$Q_{2n+1}(k) = \int_0^k t \mathrm{I}_{2n+1}(t) \, \mathrm{d}t. \tag{6.21}$$

The infinite series (6.19) for C_2 converges quickly, and we choose to truncate it after three terms. Numerical integration of these terms gives $C_2 = -(0.1401 + 0.0028 + 0.00038) \approx -0.1433$. Summing up C_1 and C_2, we find that the impulsive hydrodynamic force acting on the end-wall $y = 0$ of a semi-infinite cylinder is

$$F_{-1y} = -0.6277 \rho V R^3. \tag{6.22}$$

We now take the limit $L \to \infty$ in the general solution (6.16) and examine the surface velocity η_1 in the vicinity of the waterline along the x-axis. The free-surface velocity near the waterline $y = 0$ is given by

$$\eta_1(\tilde{x}, \tilde{y}) = \left. \frac{\partial \phi}{\partial z} \right|_{z=0} = \frac{V}{\pi} (E_1(\tilde{x}, \tilde{y}) + E_2(\tilde{x}, \tilde{y})), \tag{6.23}$$

where we introduce the dimensionless coordinates

$$(\tilde{x}, \tilde{y}) = \left(\frac{x}{R}, \frac{y}{R} \right). \tag{6.24}$$

The first contribution to the surface velocity that includes a singularity can be written as

$$E_1(\tilde{x}, \tilde{y}) = \int_0^1 \frac{\lambda}{\tilde{x}} \int_{-\pi/2}^{\pi/2} \frac{\partial}{\partial \theta} \left(\frac{1}{(\lambda^2 - 2\tilde{x}\lambda \sin\theta + \tilde{x}^2 + \tilde{y}^2)^{1/2}} \right) d\theta \, \mathrm{d}\lambda. \tag{6.25}$$

On the other hand, the second contribution is a regular function for all $\tilde{x}$ and $\tilde{y}$

$$E_2(\tilde{x}, \tilde{y}) = \frac{8}{\pi} \int_0^{\infty} \frac{\mathrm{K}'_{2m+1}(k)}{\mathrm{I}'_{2m+1}(k)} P_{2n+1}(k) \frac{\mathrm{I}_{2n+1}(k\tilde{x})}{\tilde{x}} \cos(k\tilde{y}) k^{-2} \, \mathrm{d}k. \tag{6.26}$$

Performing the above integrations, we finally find the leading-order contribution for the surface velocity η_1 near the waterline $y = 0$

$$\eta_1(\tilde{x}, \tilde{y}) = \frac{V}{\pi} \left(\log \frac{\left(\sqrt{(1-\tilde{x})^2 + \tilde{y}^2} + 1 - \tilde{x} \right) \left(\sqrt{(1+\tilde{x})^2 + \tilde{y}^2} + 1 + \tilde{x} \right)}{\tilde{y}^2} \right.$$

$$\left. - \frac{4}{\sqrt{(1-\tilde{x})^2 + \tilde{y}^2} + \sqrt{(1+\tilde{x})^2 + \tilde{y}^2}} \right) \tag{6.27}$$

again yielding a logarithmic-type singularity along the entire waterline $y = 0$, which is a local representation of the outer solution in the matched-asymptotics sense.

7. On vertical cylinders

Two problems of incompressible impulsive sloshing in vertical containers have previously been solved: vertical cylinders with circular and rectangular cross-section, respectively. To date only the leading outer solutions have been considered.

In both of these cases, there is no difference between the motions induced by sway and surge. For a circular cylinder, the impulsive hydrodynamic force will always point in the direction opposite to the direction of motion. This means that the virtual mass will be a scalar. For a rectangular cylinder the virtual mass will be a tensor, unless the cross-section is a square.

7.1. *The rectangular container*

The impulsive flow in an upright rectangular container was first investigated by Chwang & Wang (1984) and independently by Roberts (1988). Both sway and surge will generate the same type of two-dimensional flow. The fluid in the container fills a height H over the base, and the widths in the x and y directions are denoted by L_x and L_y, respectively. The initial surface velocity due to the impulsive velocity U of the container in the x direction is

$$\eta_1 = 2U \sum_{m=1}^{\infty} \frac{\cosh(k_m(L_x - x)) - \cosh(k_m x)}{k_m H \sinh(k_m L_x)}, \tag{7.1}$$

where $k_m = (m - 1/2)\pi/H$. It exhibits a logarithmic singularity of opposite sign for $x = 0$ and $x = L_x$. A similar solution was derived by Chwang & Wang (1984) for a container in constant impulsive acceleration.

In general, we have two components for the impulsive velocity U and V in the x and y directions, respectively. The surface velocity due to container motion in the y direction is found from (7.1) by the substitution $(x, L_x, U) \to (y, L_y, V)$. The hydrodynamic force can be expressed using the virtual mass tensor m_{ij} as follows

$$F_{-1i} = -m_{ij} V_j, \quad (i, j = 1, 2), \tag{7.2}$$

where $(V_1, V_2) = (U, V)$, and the subscripts 1 and 2 represent the x and y directions. The principal components of the virtual mass tensor are given by the impulsive force components

$$\frac{F_{-1x}}{mU} = -\frac{m_{11}}{m} = -4\frac{H}{L_x} \sum_{m=1}^{\infty} \frac{\tanh(k_m L_x/2)}{(k_m H)^3}, \tag{7.3}$$

and a similar expression for $F_{-1y}/(mV)$ can be found by replacing (L_x, m_{11}) with (L_y, m_{22}). Here $m = \rho L_x L_y H$ is the fluid mass inside the rectangular container.

7.2. *The hollow vertical circular cylinder*

We present here a new solution for an annular circular cylinder with its inner and outer walls moving arbitrarily in sway/surge. The radius of the outer cylinder is R_2, and it is given an impulsive velocity U in the x direction. The radius of the inner cylinder is R_1, and it is given an impulsive velocity V at an angle α to the x-axis. The undisturbed fluid depth is H.

The boundary conditions for the initial impulsive flow are

$$\phi(r,\theta,0)=0, \quad \frac{\partial\phi}{\partial z}(r,\theta,-H)=0, \tag{7.4}$$

$$\frac{\partial\phi}{\partial r}(R_1,\theta,z)=V\cos(\theta-\alpha), \quad \frac{\partial\phi}{\partial r}(R_2,\theta,z)=U\cos\theta, \tag{7.5}$$

where $r=\sqrt{x^2+y^2}$ and $\theta=\arctan(y/x)$. The complete solution for the velocity potential is

$$\phi(r,\theta,z)=\frac{2}{H}\sum_{m=1}^{\infty}\frac{V\cos(\theta-\alpha)W_m(r,R_2)-U\cos\theta W_m(r,R_1)}{k_m^3W'_m(R_1,R_2)}(-1)^{m+1}\cos(k_mz), \tag{7.6}$$

where $k_m=(m-1/2)\pi/H$ and we introduce the Wronskian

$$W_m(r,s)=\mathrm{I}_1(k_mr)\mathrm{K}'_1(k_ms)-\mathrm{K}_1(k_mr)\mathrm{I}'_1(k_ms), \tag{7.7}$$

in which I_1 and K_1 are the modified Bessel functions of order one and the prime denotes derivative with respect to the argument. We also introduce the notation

$$W'_m(r,s)=\mathrm{I}'_1(k_mr)\mathrm{K}'_1(k_ms)-\mathrm{K}'_1(k_mr)\mathrm{I}'_1(k_ms). \tag{7.8}$$

The leading-order surface velocity due to an impulsive velocity U of the cylindrical container in the x direction is

$$\eta_1=\left.\frac{\partial\phi}{\partial z}\right|_{z=-H}=-\frac{2}{H}\sum_{m=1}^{\infty}\frac{V\cos(\theta-\alpha)W(r,R_2)-U\cos\theta W(r,R_1)}{k_mW'(R_1,R_2)}, \tag{7.9}$$

implying again a logarithmic-type singularity along the inner and outer waterline contours. The case $R_1=0$ represents the interior flow inside a cylinder (Chwang & Wang 1984), whereas the case $R_2=0$ corresponds to an exterior flow outside a solid cylinder (Wang & Chwang 1989). In the case of infinitely large radii (R_1,R_2) but with finite gap $L_x=R_2-R_1$ (with $\alpha=0$ and $U=V$) it reduces to (7.1), namely the solution for the rectangular container (Chwang & Wang 1984; Roberts 1988).

The impulsive force components F_{-1x} and F_{-1y} for the general annular geometry are finite and can be expressed as

$$F_{-1x}=\frac{2\pi\rho}{H}\sum_{m=1}^{\infty}\frac{1}{k_m^3W'_m(R_1,R_2)}(V\cos\alpha[R_2W_m(R_2,R_2)-R_1W_m(R_1,R_2)] - U[R_1W_n(R_1,R_1)-R_2W_m(R_2,R_1)]), \tag{7.10}$$

$$F_{-1y}=\frac{2\pi\rho}{H}\sum_{m=1}^{\infty}\frac{V\sin\alpha}{k_m^3W'_m(R_1,R_2)}[R_2W_m(R_2,R_2)-R_1W_m(R_1,R_2)]. \tag{7.11}$$

These formulae can be made more explicit by recalling that $sW'_m(s,s)=-1/k_m$, enabling comparison with the known special cases mentioned above.

8. Wavemakers related to impulsive sloshing

A very long cylindrical container in surge motion is essentially a combination of two opposite impulsive wavemakers. This viewpoint was first proposed by Roberts (1988). Based on the wavemaker theory of Peregrine (1972), Roberts constructed

an elegant solution for impulsive sloshing in a rectangular container of finite width. From Peregrine (1972), we know that the force impulse F_{-1y} on a semi-infinite two-dimensional rectangular piston wavemaker with depth H and cross-sectional area A is

$$\frac{F_{-1y}}{(\rho AH)V} = -\frac{16}{\pi^3}\sum_{n=1}^{\infty}(2n-1)^{-3} = -0.542755, \tag{8.1}$$

where the minus sign means that the pressure impulse force on the piston is acting opposite to its motion. The mass factor (ρAH) scales the impulsive force by taking the depth as the horizontal length scale for the resulting flow. This formula can be directly compared with our result for the force impulse F_{-1y} on a triangular piston wavemaker with depth H and width $2H$ (derived in § 5.2).

$$\frac{F_{-1y}}{\rho H^3 V} = \frac{F_{-1y}}{(\rho AH)V} = -0.191662, \tag{8.2}$$

where we introduce the piston area $A = H^2$ for the triangular wavemaker piston. These two formulae give the momentum thicknesses in units of H. These are the horizontal thicknesses of local fluid cushions close to the wavemaker that effectively follow its impulsive motion. Another way of expressing this idea is to introduce virtual fluid masses: for the square piston wavemaker the virtual mass is $0.542755\rho H^3$, whereas the isosceles triangle piston with the same area has a virtual mass $0.191662\rho H^3$. The ratio between these virtual masses is roughly $3:1$. This large ratio is related to the fact that the triangle piston pushes a free-surface width that is twice as large as that pushed by the square piston of the same area and depth. At the free surface, the piston cannot exert any pressure. The greater the surface area, the more freedom there is for the fluid particles to escape from the forced horizontal piston motion. By thus diverting the forcing of the piston, the surface particles prevent the piston forcing from penetrating deeply into the fluid. This explains why the greater surface area of the triangular piston is linked to a reduced virtual mass, compared with the square piston wavemaker.

Above we have found the force impulse (6.22) for a semicircular wavemaker piston. It can be rewritten as

$$\frac{F_{-1y}}{(\rho AR)V} = -0.3996, \tag{8.3}$$

where we have introduced the wavemaker piston area $A = \pi R^2/2$, with the radius R representing the maximal fluid depth (called H in the two previous cases). The value of the force impulse on a semi-circular wavemaker piston (8.3) thus fits in nicely between the analytical results for the triangular piston (8.1) and the rectangular piston (8.2).

The explicit solution for the leading-order surface velocity induced by a planar piston-type wavemaker can be directly obtained from the rectangular container expression (7.1). Under a large-spacing approximation $k_m L_y \to \infty$, valid in the vicinity of the wall $y = 0$, it yields

$$\eta_1(y) = \frac{2V}{H}\sum_{m=1}^{\infty}\frac{\mathrm{e}^{-k_m y}}{k_m} = \frac{2U}{\pi}\sum_{m=0}^{\infty}\frac{\mathrm{e}^{-(2m+1)\pi y/(2H)}}{2m+1}. \tag{8.4}$$

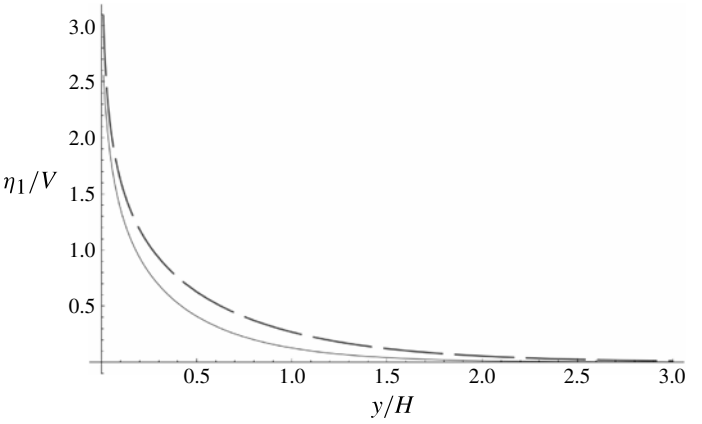

FIGURE 8. The free-surface velocity distributions for two impulsive wavemakers, as functions of the dimensionless lengthwise coordinate x/H. Solid curve: $\eta_1(H, y)/V$ along the central line of a triangular wavemaker (semi-infinite wedge container). Dashed curve: $\eta_1(y)/V$ for the rectangular wavemaker (Peregrine 1972).

The summation in (8.4) is singular at the waterline $x = 0$. Following Prudnikov, Brychkov & Marichev (1990, p. 740), the infinite sum in (8.4) reduces to

$$\eta_1(y) = -\frac{2V}{\pi} \log \tanh \frac{\pi y}{4H}. \tag{8.5}$$

This formula explicitly reveals the logarithmic singularity at the waterline $x = 0$. It was first derived by Peregrine (1972), and was confirmed by Joo, Schultz & Messiter (1990). In figure 8 we display (8.5) together with the central surface velocity $\eta_1(H, y)$ that the triangle piston wavemaker generates along the top mid-line of the wedge container. Near the piston wall, these two pistons have similar spatial variations in the surface velocity, where the triangle gives roughly a 20 % reduction of the amplitude compared with the square piston. Another important difference is that the surface velocity for the triangle piston has a much stronger decay with increasing y, compared with the square piston. This stronger spatial decay of the triangle piston shows that its forcing reaches less deeply into the fluid and explains the strong reduction in the virtual mass.

From the preceding analysis one may also construct the flow solution for a wavemaker cross-section shaped as a half circle. It has a similar logarithmic singularity in the flow velocity at the waterline, where the moving piston meets the free surface.

9. Discussion and concluding remarks

In this paper we have elucidated a distinctive class of problems relevant for sloshing in open rigid containers and coined it as incompressible impulsive sloshing. This is an essentially inertial flow in a container that suddenly changes its motion or is put into motion. Impulsive sloshing has not received much attention in comparison with the field of sloshing as a whole. Considerations of impulsive sloshing should be incorporated in the structural design of partly filled fluid tanks within seaborne or airborne vehicles and missiles.

The impulsive start of sloshing is vital for improving the understanding of initial conditions, since it is far from obvious how to bring a stagnant fluid

into an irrotational sloshing flow by moving the container walls. All initiation of incompressible free-surface flow by forced motion of a rigid container will be impulsive, no matter how smoothly it is started. This will result in forces that may be significantly different from those predicted by a traditional time-harmonic analysis. Moreover, the early impulsive flow will leave lasting signatures on the surface waves within a finite container.

To understand sloshing in a given container, one needs to know its free modes of oscillations with angular frequency ω. The linearized free-surface condition for time-periodic flow is $\partial\Phi/\partial z = K\Phi$ (at $z = 0$). Here Φ is the spatial potential (with the harmonic time dependence separated out) and $K = \omega^2/g$. An impulsive start will give $\Phi|_{z=0} = 0$ for $t = 0^+$, which leads to $\partial\eta/\partial t = 0$ at $t = 0^+$, if the flow is time periodic. This means that the undeflected state at rest is the only possible time-periodic flow with impulsive initial conditions. This trivial state has zero amplitude in the wall motion. Since no time-periodic flow can be generated by a forced motion of the walls, one has to exert work on the fluid surface itself. Unless the free modes of oscillation are triggered by some instability or resonance, they can only be started as a Cauchy–Poisson problem of one of the two types: (i) an appropriate free-surface deflection released from rest; (ii) a pressure impulse acting on the horizontal fluid surface, scaled to put the fluid into the appropriate initial velocity.

There is no natural method to trigger free harmonic oscillations by forced motion of solid boundaries that intersect with the free surface. Transient waves do not vanish in finite containers, as long as the flow is inviscid. The choice of initial conditions for harmonically forced sloshing is therefore important, in contrast to harmonic radiation of water waves in an infinite domain. Much work remains to be done on initial value problems for sloshing, and the relevance of singularities and inner expansions will continue to pose great analytical challenges. The present paper serves to address these questions, and also to present outer solutions for impulsive sloshing for some basic yet practically relevant container geometries.

We emphasize the lack of theory predicting a continuous evolution from an impulsive start to a harmonic flow inside open containers. The same dilemma also exists for the wavemaker: there is no natural way of starting a wavemaker motion in a fluid strip initially at rest Peregrine (1972), in order to establish a later time-harmonic flow driven by an oscillating wavemaker (Havelock 1929). This predicament has been investigated by Joo *et al.* (1990), who found that the surface slope at the waterline will have a discontinuous time dependence.

Some work has been published on the corresponding initial-value problem for wavemakers, see Roberts (1987), Joo *et al.* (1990) and Miles (1991). Roberts (1987) was able to show that the waterline singularity on the wavemaker for small time (physically generating a thin upward jet) can be removed if instead of an impulsive power-law generation one allows the flow to build up over an infinite amount of time, namely by exponential excitation. However, in order to address the initial value problem of an exponentially moving plate, one has to consider in a systematic manner gravity effects and therefore also include a Froude-number dependence in the linearized formulation. Nevertheless, the wave slope along the waterline remains infinite. Joo *et al.* (1990) introduced a small-time expansion using a Fourier integral method and included capillary effects in order to remove the waterline singularity. Miles (1991) also included capillary effects and found a similarity solution for the linearized initial-value problem for a piston wavemaker.

For the hydrostatic shallow-water limit of a rectangular piston wavemaker, we can give an elementary comparison between impulsive and harmonic sloshing. We compare the force amplitude F_0 in a periodic wave with the steady force of an impulsive start,

both with the same acceleration amplitude a_0. The oscillatory force $F_{0,osc}$ serves to accelerate the fluid mass within a quarter wavelength $\lambda/4$. The acceleration averaged over a quarter wavelength is $\bar{a} = (2/\pi)a_0$. This implies that $F_{0,osc} = \rho A\bar{a}\lambda/4 = \rho A a_0/k$, a result that also follows directly from pressure integration. The early impulsive wall motion generates a force $F_{0,imp}$ which is generally smaller, because it sets only a fraction of the fluid into motion, as expressed by the virtual mass $0.542755\rho AH$. This gives the ratio $F_{0,imp}/F_{0,osc} = 0.542755kH = 3.41023H/\lambda$, where λ is the wavelength of the harmonic wave generated by an oscillating wavemaker.

The requirement $H/\lambda \ll 1$ for shallow-water theory implies that $F_{0,imp}/F_{0,harm}$ is of an order smaller than one. However, one cannot conclude that the transient force after an impulsive start always remains smaller than the corresponding time-harmonic force. Joo *et al.* (1990) studied this transient start-up of an oscillating wavemaker, but they did not compute the force on the wavemaker.

In the present work we have only considered the leading-order flow of incompressible impulsive sloshing. We have studied impulsive sloshing when the container is suddenly put into a constant velocity. We have given transformations linking the case of impulsively forced velocity to impulsively forced acceleration. We have calculated the impulsive force from the fluid on the container. The associated initial free-surface flow will typically exhibits a logarithmic (integrable) singularity along the waterline contour.

When the rigid container walls put into motion are vertical, a free-surface singularity appears, defining our solution as the outer solution in the context of a matched asymptotic expansion. The challenge of developing valid inner solutions for incompressible impulsive sloshing and performing the proper matching procedure between the inner and outer solutions remains unresolved. A related matched asymptotics of the dam-break problem has been investigated by Korobkin & Yilmaz (2009).

If the Froude number of the impulsive flow in the container is smaller than one (subcritical flow), we can identify three distinct time scales for the bulk flow inside a rigid container put impulsively into motion: (i) the acoustic time scale; (ii) the incompressible impulsive time scale, which is the subject of this work; (iii) the gravitational time scale.

An example where the same three time scales can be identified is tsunami generation by sudden bottom disturbances, where the Froude number (based on the local depth) is always very small. The impulsive time scale is defined implicitly by filling the gap between the acoustic and the gravitational time scales. The fact that the impulsive time scale does not have a general explicit definition is probably the reason why the importance of incompressible impulsive free-surface flow tends to be underrated, both in connection with sloshing and the generation of tsunamis (Ward 2001).

Acknowledgements

We are grateful to E. L. Haanes for drawing the perspective sketches of the two open containers (figures 1 and 5). Thanks are also due to the Norwegian University of Life Sciences for a visiting scientist grant awarded to T.M.

REFERENCES

ABRAMOWITZ, M. & STEGUN, I. S. 1965 *Handbook of Mathematical Functions*. Dover.

CHWANG, A. T. 1978 Hydrodynamic pressures on sloping dams during earthquakes. 2. Exact theory. *J. Fluid Mech.* **87**, 343–348.

CHWANG, A. T. 1983 Nonlinear hydrodynamic pressure on an accelerating plate. *Phys. Fluids* **26**, 383–387.

CHWANG, A. T. & HOUSNER, G. W. 1978 Hydrodynamic pressures on sloping dams during earthquakes. 1. Momentum method. *J. Fluid Mech.* **87**, 335–341.

CHWANG, A. T. & WANG, K.-H. 1984 Nonlinear impulsive force on an accelerating container. *J. Fluids Engng* **106**, 233–240.

FALTINSEN, O. M. & TIMOKHA, A. N. 2009 *Sloshing*, p. 577. Cambridge University Press.

HAVELOCK, T. H. 1929 Forced surface-waves on water. *Phil. Mag.* **7, 8**, 569–576.

IBRAHIM, R. A. 2005 *Liquid Sloshing Dynamics: Theory and Applications*, p. 948. Cambridge University Press.

JOO, S. W., SCHULTZ, W. W. & MESSITER, A. F. 1990 An analysis of the initial-value wave-maker problem. *J. Fluid Mech.* **214**, 161–183.

KING, A. C. & NEEDHAM, D. J. 1994 The initial development of a jet caused by fluid, body and free-surface interaction. Part 1. A uniformly accelerated plate. *J. Fluid Mech.* **268**, 89–101.

KOROBKIN, A. & YILMAZ, O. 2009 The initial stage of dam-break flow. *J. Engng Maths* **63**, 293–308.

MILES, J. 1991 On the initial-value problem for a wave-maker. *J. Fluid Mech.* **229**, 589–601.

MILOH, T. 1980 Irregularities in solutions of nonlinear wave diffraction problem by vertical cylinder. *J. Waterway Port Coast. Ocean Div. – ASCE* **106**, 279–284.

MILOH, T., TYVAND, P. A. & ZILMAN, G. 2002 Green functions for initial free-surface flows due to 3D impulsive bottom deflections. *J. Engng Maths* **44**, 57–74.

NEEDHAM, D. J., BILLINGHAM, J. & KING, A. C. 2007 The initial development of a jet caused by fluid, body and free-surface interaction. Part 2. An impulsively moved plate. *J. Fluid Mech.* **578**, 67–84.

NEEDHAM, D. J., CHAMBERLAIN, P. G. & BILLINGHAM, J. 2008 The initial development of a jet caused by fluid, body and free surface interaction. Part 3. An inclined accelerating plate. *Quart. J. Mech. Appl. Math.* **61**, 581–614.

PEREGRINE, D. H. 1972 Flow due to a vertical plate moving in a channel. Unpublished note.

PRUDNIKOV, A. P., BRYCHKOV, YU. A. & MARICHEV, O. I. 1990 *Integrals and Series. Vol. 2, Special Functions*. Gordon & Breach.

ROBERTS, A. J. 1987 Transient free-surface flows generated by a moving vertical plate. *Quart. J. Mech. Appl. Math.* **40**, 129–158.

ROBERTS, A. J. 1988 Initial flow of liquid in an accelerating tank. *J. Engng Mech.* **114**, 175–180.

TYVAND, P. A. & STORHAUG, A. R. F. 2000 Green functions for impulsive free-surface flows due to bottom deflections in two-dimensional topographies. *Phys. Fluids* **12**, 2819–2833.

WANG, K.-H. & CHWANG, A. T. 1989 Nonlinear free-surface flow around an impulsively moving cylinder. *J. Ship. Res.* **33**, 194–202.

WARD, S. N. 2001 Landslide tsunami. *J. Geophys. Res.–Solid Earth* **106**, 11201–11215.

WESTERGAARD, H. M. 1933 Water pressures on dams during earthquakes. *Trans. Am. Soc. Civil Engng* **98**, 18–433.